




Enhancing terahertz radiation from femtosecond laser filaments using local gas density modulation

Haicheng Xiao ¹, Shengfeng Wang,¹ Yan Peng ^{1,*}, Daniel M. Mittleman ², Jiayu Zhao,¹ Zuanming Jin,¹ Yiming Zhu,^{1,*} and Songling Zhuang¹

¹*Terahertz Technology Innovation Research Institute, Terahertz Spectrum and Imaging Technology Cooperative Innovation Center, Shanghai Key Lab of Modern Optical System, University of Shanghai for Science and Technology, Shanghai 200093, People's Republic of China*

²*School of Engineering, Brown University, Providence, Rhode Island 02912, USA*



(Received 19 April 2021; accepted 22 June 2021; published 16 July 2021)

We present a method to enhance the terahertz (THz) wave radiation from a femtosecond laser-induced plasma filament by controlling the local gas density within the filament. We develop a theoretical model for THz generation from a laser-induced air plasma filament and the subsequent propagation process, to account for a varying local gas density. By adjusting the local gas density along the filament, the transient current distribution along the filament and the resulting coherent superposition of terahertz waves can be controlled. The location of the gas jet nozzle and the relative phase between multicolor light fields both affect the transient current distribution and thus the strength of the generated THz field. Compared with the conventional terahertz generation by a two-color filament in a homogeneous gas, a three-color filament can realize an increase by 6.12 times in the generated THz pulse energy, with optimized local gas density modulation. Our results suggest that the THz amplification via local gas density modulation can be further improved with well-designed multicolor pulses.

DOI: [10.1103/PhysRevA.104.013517](https://doi.org/10.1103/PhysRevA.104.013517)

I. INTRODUCTION

The unique properties of terahertz waves have inspired applications prospects in many fields, such as astronomy, atmospheric and environmental sensing, communications, biomedicine, counterterrorism, security inspection, material science, etc. [1–5]. Therefore, the design of high-power versatile THz sources has become a focus of much research. There are many ways to generate terahertz waves, including optical rectification using nonlinear crystals (such as LiNbO₃) [6,7], photoconductive antennas [8,9], electron accelerators [10], and laser-induced air plasma [11–13]. Compared with other methods, the method of laser-induced air plasma has gained popularity due to the ease of implementation, and also to the ability to scale to high energy because of the lack of laser damage threshold in gaseous media. This laser-induced terahertz source has also shown promise for remote generation, thereby avoiding the strong absorption of terahertz radiation by atmospheric water vapor [14–16].

In 1993, Hammer *et al.* ionized air with single-color laser, and obtained multiband electromagnetic radiation containing terahertz waves [12]. In 2000, Cook *et al.* found that focusing both the fundamental ω and its second harmonic 2ω on the target gas could produce a much stronger THz signal, due to the left-right asymmetry of the peak electric field of the

coherently superposed light fields. As a result, this method achieves a typical conversion efficiency of 10^{-5} – 10^{-4} [17].

The radiated THz field originates from the gas ionization and the subsequent transient current induced in the plasma filament by the asymmetric two-color laser electric field [13,18]. As the length of the laser filament increases (>10 mm), the transient current formed at different positions along the two-color laser filament will vary significantly. This effect arises due to the dispersion of the plasma, which leads to a walk-off between the ω and 2ω beams, resulting in a change in their relative phase. As a result, different sections of the filament radiate THz waves with different amplitude and phase [19,20]. Since the total radiated THz signal consists of a superposition of the fields radiated by all points along the filament, this clearly affects the overall terahertz radiation intensity [21,22]. At present, the only method for manipulating this effect is to adjust the time delay (relative phase) of the two laser fields before they reach the focal point and initiate the plasma generation [21,22]. A method to adjust the relative phases of the laser fields within the filament would provide a valuable additional parameter for optimizing the THz generation efficiency.

Here, we present a method for adjusting the local THz generation conditions by controlling the local gas density within the femtosecond laser filament. By establishing a model of terahertz wave radiation and propagation, we investigate the effects of the local gas density of the filament on the generated THz energy. Our model predicts that this method can result in dramatic improvements in the THz generation mechanism.

*Corresponding authors: py@usst.edu.cn; ymzhu@usst.edu.cn

II. MODEL

We describe the laser-induced filament in an axially symmetric geometry. Thus, we use a two-dimensional model to simplify the analysis. We introduce a cylindrical coordinate system, where the z axis is the propagation axes of the laser beam, the r axis is the radial coordinate, and the coordinate origin corresponds to the geometric midpoint of the filament.

We assume that the multicolor lasers used in the model are linearly polarized, all parallel to each other. To treat the general case, we include three laser fields, corresponding to the fundamental field (at frequency ω), together with its second and third harmonics. Assuming that all of these fields are short pulses with Gaussian envelopes, the coherently superposed three-color laser electric field ($\omega + 2\omega + 3\omega$) can be written as [14]

$$\begin{aligned} E_l(t) = & E_1 \exp\left(-\frac{t^2}{T_1^2}\right) \cos(\omega t) \\ & + E_2 \exp\left(-\frac{t^2}{T_2^2}\right) \cos(2\omega t + \theta_2) \\ & + E_3 \exp\left(-\frac{t^2}{T_3^2}\right) \cos(3\omega t + \theta_3), \end{aligned} \quad (1)$$

where E_1 , E_2 , and E_3 are the amplitudes of the ω , 2ω , and 3ω fields, T_1 , T_2 , and T_3 are their pulse widths, and the phases θ_2 and θ_3 are the relative phase between ω and 2ω and the relative phase between ω and 3ω , respectively. The process of laser ionizing gas can be described by the Ammosov-Delone-Krainov model [23,24], in which the evolution of the electron density $N_e(t)$ can be derived from [14]

$$dN_e(t) = W_{\text{ADK}}(t)[N_g - N_e(t)]dt. \quad (2)$$

Here, $W_{\text{ADK}}(t)$ is the ionization rate, and N_g is the density of gas molecules. After the gas molecules are ionized, the liberated electrons are driven by the laser field to form a transient current $J(t)$, which can be expressed as [25]

$$\frac{dJ(t)}{dt} = \frac{e}{m_e} N_e(t) E_l(t) - \nu_e J(t), \quad (3)$$

where ν_e is the electron collision frequency, e is the elementary charge, and m_e is the electron mass. This transient current generates a THz field according to $E_{\text{THz}} \propto dJ/dt$. The spectrum of the resulting terahertz wave can be obtained by Fourier transform of the time derivative of $J(t)$. The time-domain wave form of the terahertz radiation can be obtained by filtering the pump laser frequency from this spectrum, followed by an inverse Fourier transform.

The transient current elements produced by the laser field inside the filament can be regarded as a combination of source points for the generated THz field, arrayed along a line. Here, we assume that these transient currents at each point along the line are independent of each other. In this case, the total field radiated by the filament can be regarded as the superposition of the fields radiated by the transient currents at each point. A key issue is that the THz electric field generated at each point along the filament is different. As mentioned above, when the multicolor laser propagates along the filament, the relative phase between the different frequency components changes, due to dispersion. Taking the three-color field as an

example, the relative phase shifts between ω and 2ω , 3ω can be expressed as

$$\theta_2(z) = \theta_2(z_0) + k_\omega \int_{z_0}^z [n_\omega(z') - n_{2\omega}(z')] dz', \quad (4)$$

$$\theta_3(z) = \theta_3(z_0) + k_\omega \int_{z_0}^z [n_\omega(z') - n_{3\omega}(z')] dz', \quad (5)$$

where k_ω is the wave number of the fundamental wave, and n_ω , $n_{2\omega}$, and $n_{3\omega}$ are the refractive indices of the filament at frequencies ω , 2ω , and 3ω respectively. In order to obtain the total THz radiation in the far field, we must consider the variation of THz radiation generated by each point along the filament due to this dispersive effect. In addition, we must also include the propagation phase of THz wave generated at each point, since the filament can be long compared to the THz wavelength. Finally, we also include the attenuation of the THz wave due to propagation in the plasma filament.

Assuming that the terahertz wave propagates from $P_0(z_0, r_0)$ to $P_1(z_1, r_1)$ in the filament, its phase change can be expressed as

$$\varphi(\omega_{\text{THz}}, p_1) = \varphi(\omega_{\text{THz}}, p_0) + \int_{z_0}^{z_1} \frac{k_{\text{THz}} n_{\text{THz}}(\omega_{\text{THz}}, z, r)}{\cos \phi} dz, \quad (6)$$

where k_{THz} is the THz wave number, $n_{\text{THz}}(\omega_{\text{THz}}, z, r) = \sqrt{1 - \omega_p^2(z, r)/\omega_{\text{THz}}^2}$ is the refractive index of the THz wave in the filament obtained from the Drude model, and $\omega_p = \sqrt{e^2 N_e / m_e \epsilon_0}$ is the plasma frequency. We assume that the electron density distribution in the filament is radially symmetric, given by $N_e(r) \sim \cos^2(\pi r / 2r_p)$, where r_p is close to the filament radius. The factor of $\cos \phi$ in Eq. (6) arises from the fact that the wave vector of the THz wave need not be parallel to the z axis, but instead can propagate at an angle ϕ .

To account for attenuation of the THz signal, we can compute the loss factor, which applies for all frequencies above the plasma frequency, $\omega_{\text{THz}} > \omega$. The characteristic attenuation distance for waves in a plasma above the plasma frequency is $L_a(\omega_{\text{THz}}, z, r) \approx 2c(\omega_{\text{THz}}^2 + \nu_e^2)/(\omega_p^2 \nu_e)$ [13,26]. Writing the projection of the paraxial propagation distance $D(z)$ on the optical axis as $D'(z) = D(z) \cos \phi$, the attenuation coefficient can be expressed as

$$K(\omega_{\text{THz}}, z) = \begin{cases} \exp\left[\int_0^{D'(z)} -\frac{D'(z)-z}{L_a(\omega_{\text{THz}}, z, r) \cos \phi} dz\right], & \omega_{\text{THz}} \geq \omega_p \\ 0, & \omega_{\text{THz}} < \omega_p \end{cases} \quad (7)$$

Combining Eqs. (2)–(7), the far-field terahertz $E_{\text{THz}}^{\text{Far}}$ can be expressed as an integral over the length of the filament:

$$\begin{aligned} E_{\text{THz}}^{\text{Far}}(\omega_{\text{THz}}) = & \int^{\text{filament}} E_{\text{THz}}(\omega_{\text{THz}}, z) K(\omega_{\text{THz}}, z) \\ & \times \exp[j\varphi(\omega_{\text{THz}}, z)] dz. \end{aligned} \quad (8)$$

A key idea of this work is the addition of a gas-puff nozzle near the filament, which would enable the modulation of the local gas density. We can incorporate this effect into our model through a variation in the gas density distribution $N_g(r, z)$, which can now depend on the z coordinate. The gas density

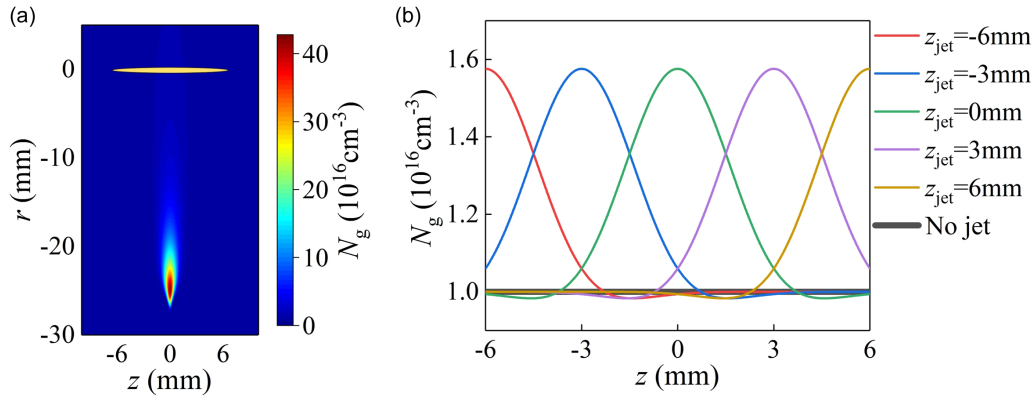


FIG. 1. (a) Spatial density distributions of the gas formed by jet nozzle (the yellow bar stands for the filament). (b) The gas density distribution at the filament with different nozzle position z_{jet} .

distribution from a nozzle can be estimated using a ballistic transport model [27], which is expressed as

$$N_g(z, r) = \frac{N}{\pi(r\theta_d)^2} \exp\left[-\frac{z^2 + (R_n - r\theta_t)^2}{(r\theta_d)^2}\right] I_0\left[\frac{2z(R_n - r\theta_t)}{(r\theta_d)^2}\right], \quad (9)$$

where N is the line density of the airflow, R_n is the nozzle radius, θ_d is the divergence angle of gas escaping from the nozzle, θ_t is the nozzle tilt angle, and I_0 is the Bessel function.

III. SIMULATION RESULTS AND ANALYSIS

As a first step in implementing the model described above, we consider a two-color laser filament ($\omega + 2\omega$), $\omega = 800$ nm as an example. We assume that the energy of the two-color laser pulse is $14 \mu\text{J}$, where the energy ratio of 2ω pulse to ω pulse is 0.2. The laser intensity is $2.8 \times 10^{18} \text{ W/m}^2$, which is close to the saturation of the first ionization, so we don't consider multiple ionization here. The filament length is 12 mm, and the filament radius is $80 \mu\text{m}$. The initial nitrogen gas density of the environment is $N_g = 1 \times 10^{16} \text{ cm}^{-3}$; the jet nozzle with radius $R_n = 1$ mm and divergence angle of gas $\theta_d = 6^\circ$ is located 30 mm below the filament. This modulates the local gas density of the filament, as shown in Fig. 1(a). By varying the abscissa z_{jet} of the nozzle position relative to the filament center, the density distribution of the gas in different sections of the filament can be modulated. As shown in Fig. 1(b), the entire modulation range of the nozzle at the filament is about 6 mm, and the peak value of the gas density after modulation is about $1.6 \times 10^{16} \text{ cm}^{-3}$.

Next, we analyze the effect of changing the local gas density on the transient current distribution induced in the filament. When the multicolor laser propagates forward in the filament, the dispersion of the plasma causes the change of relative phase among the different frequency components, resulting in changes in the transient current at each point along the filament. When the nozzle changes the local gas density, the points with increased local gas density will have higher electron density and larger transient current; that is, these points will radiate terahertz waves with higher central frequency and greater amplitude. As shown in

Fig. 2(a), for example, the two-color filament with the initial relative phase $\theta_2 = 0.75\pi$, we see that the transient current increases in the filament area corresponding to the nozzle positions.

We also need to consider the coherent superposition of terahertz waves radiated by each point. According to Eq. (8), this can be computed by integrating along the filament. However, to facilitate our calculations, we convert this integral to a discrete sum over points along the filament, with separation of $50 \mu\text{m}$ (much less than any wavelength in the THz pulse). For a 12-mm filament length, we therefore have 241 discrete points in our summation, which provides a good approximation to the integral given in Eq. (8), but with much less computational overhead. We can obtain useful physical insight by looking at the relative phases of the THz signals from some of these discrete source points. Figures 2(c)–2(h) display a few of the THz wave forms (from nine particular source points out of the 241 in our calculation, with a spacing of 1.5 mm) which arrive at a particular location in the far field (corresponding to $z = 49.81$ mm, $r = 4.36$ mm in our cylindrical coordinate system defined above). These computations take into account all of the effects noted above: the relative phase of the w and $2w$ fields which vary along the filament length, the strength and phase of the resulting transient current, and the subsequent propagation of the THz field through the filament to the chosen field point. Figure 2(c) shows the result when there is no gas nozzle near the filament (so the gas density distribution is independent of z), while Figs. 2(d)–2(h) show the results when a gas nozzle is present, situated at several different locations along the filament [as in Fig. 1(b)].

As compared to the no-jet case [Fig. 2(c)], the amplitudes of the terahertz waves radiated from points along the filament change with the jet nozzle position; in addition, their relative coherence changes strongly with jet nozzle position. Because the phase velocity of terahertz waves with different frequencies are different, a longer THz propagation distance in the filament results in a greater degree of decoherence, which has a very significant impact on the total THz signal that results from the superposition of these wavelets. In particular, when the nozzle position z_{jet} is close to the front of the filament [e.g., Fig. 2(d)], the decoherence phenomenon between terahertz waves radiated by each point is more significant due to the

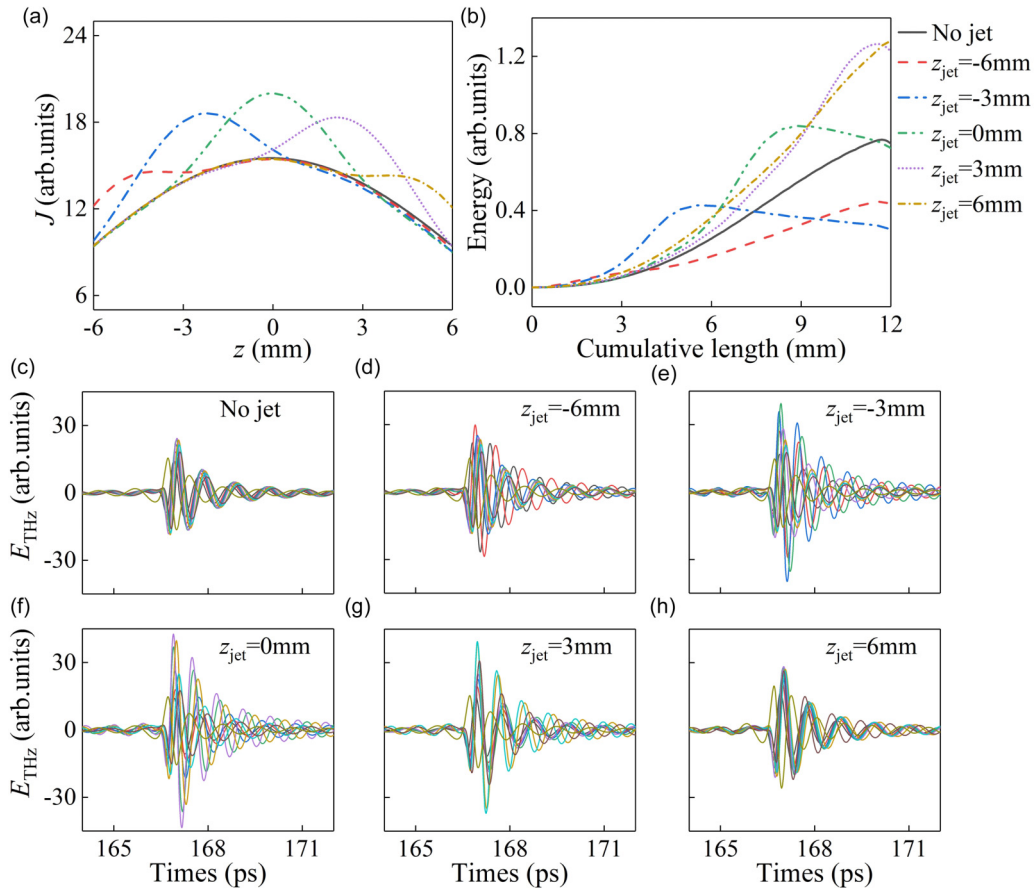


FIG. 2. (a) Transient current distribution of filament and (b) cumulative THz energy change and (c)–(h) superposition of THz electric field of each point at the measurement point under different z_{jet} .

longer propagation of the THz signal to the measurement point. Conversely, when the nozzle position z_{jet} is close to the end of the filament [e.g., Fig. 2(h)], the decoherence phenomenon is suppressed. Figure 2(b) shows the relationship between the cumulative terahertz energy computed by summing (superposition) of all the points along the filament at this measurement point and the corresponding cumulative length of filament. The closer the nozzle position z_{jet} to the end of filament, the weaker the influence of decoherence, and thus the higher the accumulated THz energy in the far field. Although the overall transient current is higher when z_{jet} is located in the middle of filament [Fig. 2(a)], the highest accumulated energy reaching the measurement point occurs when z_{jet} is located near the end of the filament [see Fig. 2(b)]. We conclude that, compared with the enhancement effect caused by increasing local transient current, the coherence between the terahertz waves radiated by each point has a bigger influence. We note that, even for this simple situation, the addition of a gas nozzle near the end of the filament can lead to nearly twice as much generated THz energy.

As a next step, we analyze the effect of the initial relative phase of the multicolor laser pulses in combination with the local gas modulation. For the usual case of homogeneous gas, the initial relative phase of multicolor laser will affect the transient current distribution along the filament [28]. Taking into account the dispersive effects noted above, this initial

phase evolves along the length of the filament, resulting in a change in the magnitude of the transient current distribution. As shown in Figs. 3(b)–3(d), when $\theta_2 = 0.5\pi$, the transient current peak is located at the front of the filament. When $\theta_2 = 0.75\pi$, the transient current peak is in the middle of filament, and the overall transient current intensity is the highest. When $\theta_2 = \pi$, the transient current peak is at the end of the filament, and the overall strength of the transient current of the filament is similar to $\theta_2 = 0.5\pi$. When the jet nozzle is applied, the transient current increases in the filament area corresponding to the nozzle position z_{jet} . Thus, under different initial relative phases, the transient current distribution of the filament is changed in different ways as a function of the jet nozzle position z_{jet} . This has an impact on the total generated THz energy, as shown in Fig. 3(a).

It is worth noting that, compared with the case of relative phase $\theta_2 = \pi$, the transient current increase in the filament formed when $\theta_2 = 0.5\pi$ is larger when the nozzle is applied at the front of the filament. However, the decoherence effect plays an important role when the nozzle is applied at the front of the filament. Thus, when z_{jet} is located in the front of filament, the total terahertz energy is lower when $\theta_2 = 0.5\pi$ than when $\theta_2 = \pi$ [Fig. 3(a)]. As a result of the interplay between these effects, different relative phase θ_2 causes different trends in the THz energy with the jet nozzle position z_{jet} . The

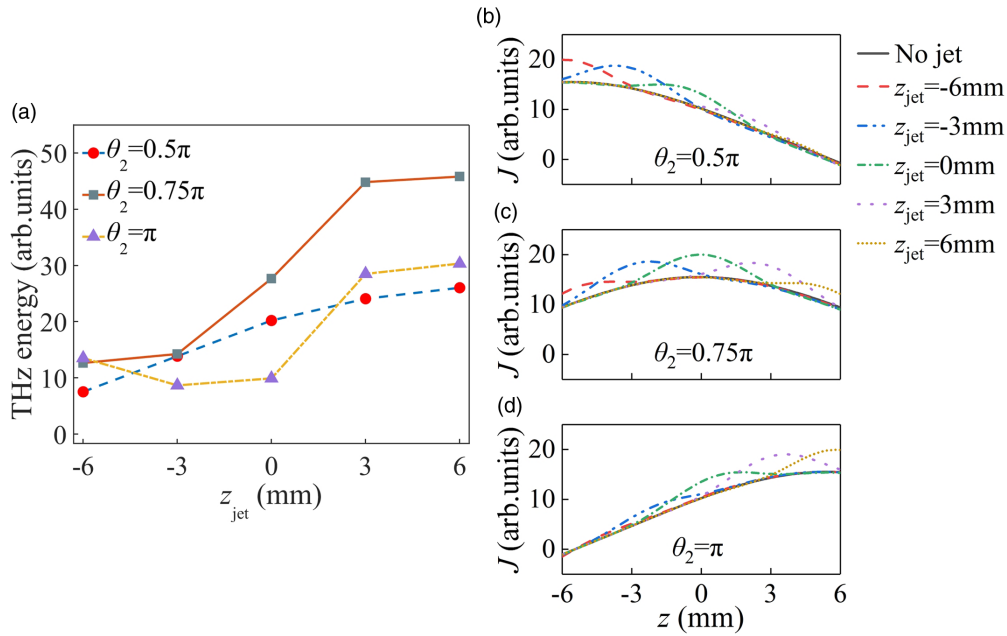


FIG. 3. (a) Evolution of terahertz radiation energy and (b)–(d) the distribution of filament transient current with z_{jet} under different initial relative phases.

THz energy reaches its largest value for the initial relative phase $\theta_2 = 0.75\pi$.

We can also investigate the influence of jet nozzle position on the spatial distribution of THz intensity. The simulation results (Fig. 4) show that after a certain distance (~ 50 mm) propagated in the air, the THz radiation from the filament presents a forward cone-shaped intensity spatial distribution, resulting from the plasma attenuation and the coherent superposition in the far field of the THz waves radiated by each point along the filament. The intensity distribution changes as expected with the jet nozzle position: when z_{jet} moves from the front to the rear of the filament, the overall radiation intensity gradually increases, and the radiation cone angle shows a trend of first increasing and then decreasing [Fig. 4(g)]. When the nozzle is located at the rear of the filament, the angle with the strongest THz radiation is about 5° . Figure 4(h) is a comparison of the total terahertz energy with and without jet nozzle. When z_{jet} is at the front of filament, the total terahertz energy is about half of the terahertz energy without nozzle. As z_{jet} moves towards the end of filament, the total terahertz energy gradually increases, reaching 1.86 times the total terahertz energy of filament without nozzle.

We further compare the case of local gas density modulation with the overall ambient gas density modulation. The increase of gas density causes an increase of the electron density in the filament. Although the transient current increases correspondingly, it can be seen from the geometric relationship and Eq. (6) that the increase of electron density impacts the phase difference between terahertz waves from different points along the filament. As a result, when the ambient gas density increases, the decoherence between the terahertz waves from each point increases. This limits the increase of the far-field terahertz radiation intensity. However, in the filament with local gas density modulation, only the local

electron density is changed, and the coherence between terahertz radiation from different source points is less affected. Thus, we anticipate that the use of local control of the gas density with a nozzle is superior to varying the ambient gas density as a tool for increasing the far-field terahertz intensity.

As shown in Fig. 5(a), as the ambient gas density increases uniformly, the terahertz energy radiated also shows a trend of rising first and then falling, reaching its maximum when the ambient gas density is $3 \times 10^{16} \text{ cm}^{-3}$. This is only 1.65 times the signal from the initial case without jet. The terahertz energy radiated by the two-color filament modulated by the local gas density reaches the optimal value when the gas density peak value is $1.58 \times 10^{16} \text{ cm}^{-3}$, which is 1.87 times the signal from the filament in the uniform gas with the initial gas density ($1 \times 10^{16} \text{ cm}^{-3}$), so the enhancement effect is better than that of the overall ambient gas density modulation. However, if the jet strength is further enhanced, as the gas density peak continues to increase, the attenuation effect of the plasma [Eq. (7)] on the terahertz wave also increases rapidly, so the terahertz radiation energy gradually decreases.

We now explore the extension of our model to the case of a three-color laser-induced filament. Compared with the two-color laser filament, three-color laser filament has two main differences: (1) the electric field of three-color laser has stronger asymmetry and faster electric field oscillation, so the transient currents induced by this field are larger, resulting in stronger terahertz radiation; (2) the evolution of the relative phase between multicolor lasers along the filament will accelerate with the increase of electron density, resulting in a more pronounced change in the transient current distribution (specifically, the peak transient current moves to the front of filament). The transient current distribution of three-color laser filament is affected by both θ_2 and θ_3 . Therefore, compared with the two-color case, the variation of the transient current along the filament in the three-color case is relatively

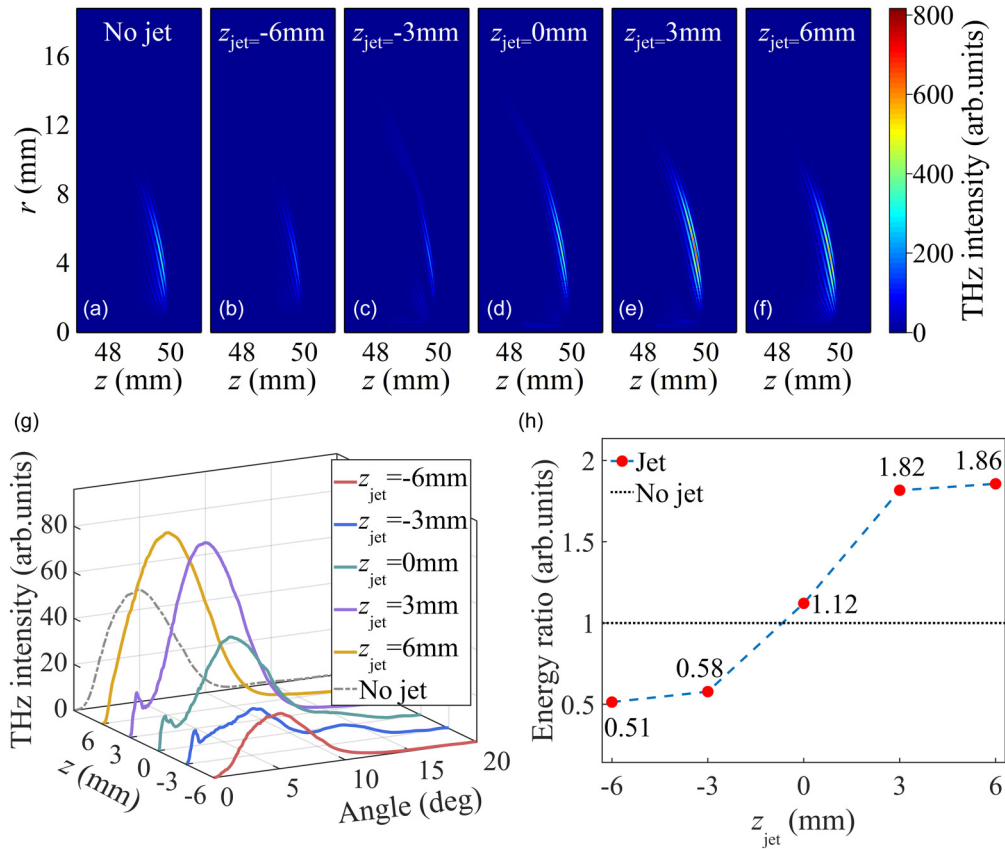


FIG. 4. (a) Spatial distribution of THz intensity of two-color filament without nozzle and (b)–(f) with nozzle, (g) angular distributions of THz intensity, and (h) comparison of THz energy of filament without nozzle and THz energy of filament without nozzle under different z_{jet} (set THz energy of filament without nozzle as 1).

slow (that is, the difference among transient current values for each source point is smaller for the three-color case).

As a result of these considerations, it is not surprising that the terahertz radiation energy from a three-color laser filament varies with the gas density differently from that from a two-color laser filament. Numerical calculations show that when the other parameters are the same, the three-color laser filament ($\omega + 2\omega + 3\omega$) with a fundamental wavelength of 800 nm at the initial relative phase of $\theta_2 = 0.75\pi$ and $\theta_3 = 1.2\pi$ has a similar transient current distribution with the two-color laser filament with an initial relative phase of $\theta_2 = 0.75\pi$; specifically, the peak value of the filament transient current is located in the middle of the filament. So, we use the three-color laser filament with these parameters for the subsequent calculations. We also assume that the energy ratio between the ω , 2ω , and 3ω pulses in the three-color laser is 1:0.2:0.05.

The results of these simulations, shown in Fig. 5(b), allow us to draw several conclusions. First, in the case of local gas density modulation at the rear of filament, when the electron density and transient current increase, the decoherence between terahertz waves radiated by each point of filament is less significant. As a result, the strength of the terahertz radiation increases with increasing local transient current modulation. This is more favorable for high-power terahertz generation in comparison with a two-color laser filament.

Second, when the ambient gas density increases uniformly, the electron density along the filament increases accordingly, and the decoherence between the terahertz waves from source points at the front and the rear of the filament becomes a more significant concern. Compared with the two-color laser filament, where the transient current values at the front and the rear of the filament are more similar, the signal from the three-color laser filament exhibits a greater impact from the decoherence effect. Therefore, the terahertz radiation energy from the three-color laser filament decreases more rapidly as the ambient gas density increases.

Here, we also presented the change of electron density under two-color and three-color laser cases, as shown in Figs. 5(c) and 5(d). It can be seen that the existence of jet only affects the maximum value but not the rising law of N_e , where the electron density in the case of the three-color laser increases slightly faster than that of the two-color laser.

Finally, we investigate the effect of the distance between filament and nozzle (ordinate r_{jet}) on terahertz radiation energy. We set the abscissa of the nozzle at $z_{\text{jet}} = 6$ mm. Figure 6(a) shows the effect of the nozzle's ordinate r_{jet} on the local gas density in the filament. When the nozzle is close to the filament, the local peak gas density is higher and the peak is narrower. That is to say, the ordinate r_{jet} of the nozzle affects both the modulation range and intensity of the local gas density. This modulation affects both the attenuation of the THz wave due to plasma absorption and the decoherence

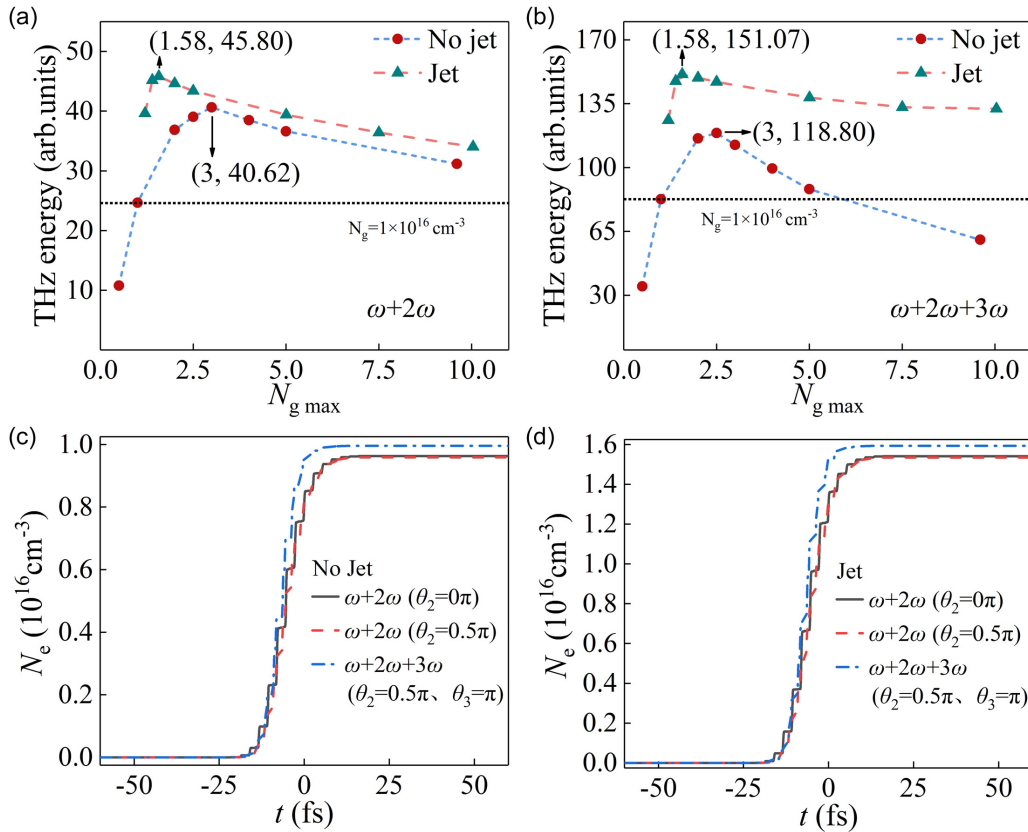


FIG. 5. (a) Two-color laser filament and (b) three-color laser filament: evolution of terahertz radiation energy with gas peak density for filament without jet nozzle and filament with jet nozzle (the dotted line is the terahertz radiation energy of filament without nozzle under the initial gas density). Panels (c) and (d) are electron density versus time without and with jet.

between terahertz waves radiated by different points along the filament. As a result of these effects, varying r_{jet} leads to a nonmonotonic variation of the strength of the far-field THz radiation. We find that there is an optimal value for the vertical distance between the filament and the jet nozzle. With the parameters used in this example, this optimal distance is 30 mm, as shown in Fig. 6(b). We predict that the optimal far-field THz energy from a two-color filament modulated by a jet nozzle is 1.87 times larger than the energy generated

with no jet, and that of a three-color filament modulated by jet nozzle is 6.12 times larger. It may be possible to improve these values even further, through optimization of the various experimental parameters.

IV. CONCLUSION

In this paper, we establish a physical model to describe THz generation from a femtosecond laser air plasma, and

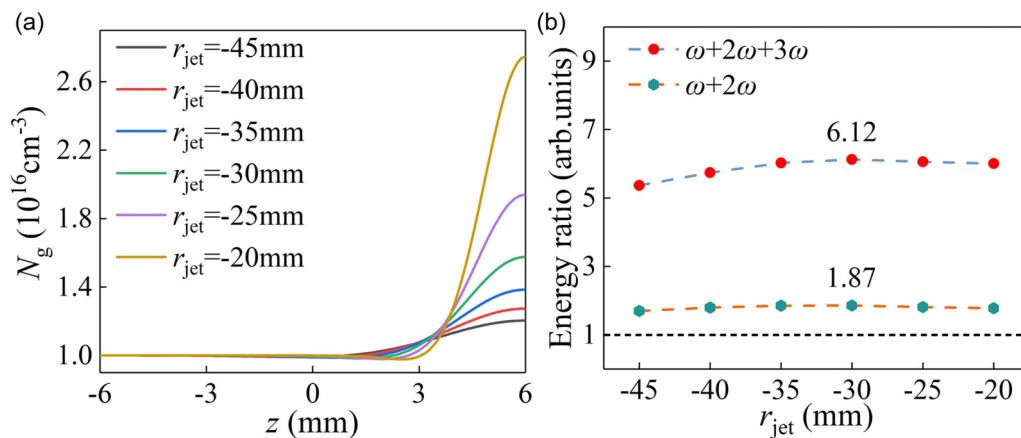


FIG. 6. (a) The distribution of gas density at the filament position for different values of r_{jet} , and (b) the evolution of the total terahertz energy measured in the far field (integrated over the entire far-field region) as a function of the nozzle's ordinate r_{jet} . Here, we normalize the result to the terahertz energy from a two-color laser filament with no gas nozzle.

present a method for optimizing this process using local gas density modulation. The model accounts for the effects of the location of a gas jet nozzle, the relative phase of multicolor laser pulses, and gas density in the plasma filament.

Our results emphasize the importance of maintaining the coherence between THz wavelets radiated by various parts of the filament in optimizing the yield of THz radiation in the far field. The calculation suggests that optimizing the parameters of a three-color filament using local gas density modulation can result in an increase in the energy of

the terahertz pulse by a factor of 6.12 times compared with the standard two-color configuration. This enhancement in the THz signal via local gas density modulation can be further improved with well-designed multicolor pulses. Although we ignore distortions in the rear part of the temporal pulse profile due to plasma defocusing [29], which is what we should improve in the future, these results are of great significance to explain the physical process of laser filamentation and to optimize the efficiency of conversion from optical to THz fields.

-
- [1] B. Fischer, M. Hoffmann, H. Helm, G. Modjesch, and P. U. Jepsen, *Semicond. Sci. Technol.* **20**, S246 (2005).
- [2] P. Han and X. Zhang, *Meas. Sci. Technol.* **12**, 1747 (2001).
- [3] L. Ho, M. Pepper, and P. Taday, *Nat. Photon.* **2**, 541 (2008).
- [4] M. Tonouchi, *Nat. Photon.* **1**, 97 (2007).
- [5] K. Sengupta, T. Nagatsuma, and D. M. Mittleman, *Nat. Electron.* **1**, 622 (2018).
- [6] Y.-S. Lee, T. Meade, V. Perlin, H. Winful, T. Norris, and A. Galvanauskas, *Appl. Phys. Lett.* **76**, 2505 (2000).
- [7] J. Hebling, K. Yeh, M. C. Hoffmann, and K. A. Nelson, *IEEE J. Sel. Top. Quantum Electron.* **14**, 345 (2008).
- [8] C. W. Berry, M. R. Hashemi, and M. Jarrahi, *Appl. Phys. Lett.* **104**, 081122 (2014).
- [9] P. R. Smith, D. H. Auston, and M. C. Nuss, *IEEE J. Quantum Electron.* **24**, 255 (1988).
- [10] G. L. Carr, M. C. Martin, W. R. McKinney, K. Jordan, G. R. Neil, and G. P. Williams, *Nature (London)* **420**, 153 (2002).
- [11] H. Hamster, A. Sullivan, S. Gordon, and R. W. Falcone, *Phys. Rev. E* **49**, 671 (1994).
- [12] H. Hamster, A. Sullivan, S. Gordon, W. White, and R. W. Falcone, *Phys. Rev. Lett.* **71**, 2725 (1993).
- [13] K. Y. Kim, A. J. Taylor, J. H. Glowina, and G. Rodriguez, *Nat. Photon.* **2**, 605 (2008).
- [14] H. G. Roskos, M. D. Thomson, M. Kreß, and T. Löffler, *Laser Photon. Rev.* **1**, 349 (2007).
- [15] C. D'Amico, A. Houard, M. Franco, B. Prade, A. Mysyrowicz, A. Couairon, and V. T. Tikhonchuk, *Phys. Rev. Lett.* **98**, 235002 (2007).
- [16] Y. Chen, T.-J. Wang, C. Marceau, F. Théberge, M. Châteauneuf, J. Dubois, O. Kosareva, and S. L. Chin, *Appl. Phys. Lett.* **95**, 101101 (2009).
- [17] D. J. Cook and R. M. Hochstrasser, *Opt. Lett.* **25**, 1210 (2000).
- [18] P. G. d. A. Martínez, I. Babushkin, L. Bergé, S. Skupin, E. Cabrera-Granado, C. Köhler, U. Morgner, A. Husakou, and J. Herrmann, *Phys. Rev. Lett.* **114**, 183901 (2015).
- [19] L. Zhang, S. Zhang, R. Zhang, T. Wu, Y. Zhao, C. Zhang, and X. C. Zhang, *Opt. Express* **25**, 32346 (2017).
- [20] A. Nguyen, K. J. Kaltenecker, J. C. Delagnes, B. Zhou, E. Cormier, N. Fedorov, R. Bouillaud, D. Descamps, I. Thiele, and S. Skupin, *Opt. Lett.* **44**, 1488 (2019).
- [21] M. Kress, T. Löffler, S. Eden, M. Thomson, and H. G. Roskos, *Opt. Lett.* **29**, 1120 (2004).
- [22] K. Y. Kim, J. H. Glowina, A. J. Taylor, and G. Rodriguez, *Opt. Express* **15**, 4577 (2007).
- [23] P. B. Corkum, *Phys. Rev. Lett.* **71**, 1994 (1993).
- [24] S. C. Rae and K. Burnett, *Phys. Rev. A* **46**, 1084 (1992).
- [25] V. A. Andreeva, O. G. Kosareva, N. A. Panov, D. E. Shipilo, P. M. Solyankin, M. N. Esaulkov, P. González de Alaiza Martínez, A. P. Shkurinov, V. A. Makarov, L. Bergé, and S. L. Chin, *Phys. Rev. Lett.* **116**, 063902 (2016).
- [26] E. Constant, D. Garzella, P. Breger, E. Mével, C. Dorrer, C. Le Blanc, F. Salin, and P. Agostini, *Phys. Rev. Lett.* **82**, 1668 (1999).
- [27] D. Mosher, R. J. Comisso, and B. V. Weber, in *Proceedings of the 12th IEEE International Pulsed Power Conference, Monterey, CA, USA*, Digest of Technical Papers (IEEE, New York, 1999), p. 1078.
- [28] Y. S. You, T. I. Oh, and K. Y. Kim, *Phys. Rev. Lett.* **109**, 183902 (2012).
- [29] A. Nguyen, P. González de Alaiza Martínez, J. Déchard, I. Thiele, I. Babushkin, S. Skupin, and L. Bergé, *Opt. Express* **25**, 4720 (2017).